Global and Planetary Change 123 (2014) 44–54

Contents lists available at ScienceDirect

Global and Planetary Change

journal homepage: www.elsevier.com/locate/gloplacha

Edifice growth and collapse of the Pliocene Mt. Kenya: Evidence of large scale debris avalanches on a high altitude glaciated volcano

J.M. Schoorl [a,*], A. Veldkamp [b], L. Claessens [a,c], W. van Gorp [a], J.R. Wijbrans [d]

[a] Soil Geography and Landscape Group, Wageningen University, P.O. Box 47, 6700 AA Wageningen, The Netherlands
[b] Faculty ITC, University of Twente, P.O. Box 217, 7500 AE Enschede, The Netherlands
[c] International Crops Research Institute for the Semi-Arid Tropics (ICRISAT), P.O. Box 39063, 00623 Nairobi, Kenya
[d] Department of Earth Science, VU University, De Boelelaan 1085, 1081 HV Amsterdam, The Netherlands

ARTICLE INFO

Article history:
Received 19 February 2014
Received in revised form 16 September 2014
Accepted 15 October 2014
Available online 24 October 2014

Keywords:
$^{40}Ar/^{39}Ar$ geochronology
lahar
phonolite
volcanic debris avalanche
Kenya Rift valley
Pliocene
Mt. Kenya

ABSTRACT

The cyclic growth and destruction of the Late Cenozoic Stratovolcano Mt. Kenya have been reconstructed for its southeastern segment. At least three major debris avalanche deposits have been reconstructed and dated. The oldest deposits indicate an edifice collapse around 4.9 Ma ($^{40}Ar/^{39}Ar$), followed by a larger event around 4.1 Ma ($^{40}Ar/^{39}Ar$). The last and best preserved debris avalanche deposit, with still some morphological expression covering the whole 1214 km^2 SE sector, occurred around 2.83 Ma ($^{40}Ar/^{39}Ar$). This very large debris avalanche event must have truncated the whole top of Mt. Kenya. Of the original typical hummocky relief, only local topographical depressions are still best visible and preserved. Using known geometric empirical parameters of the 3 preserved debris-avalanche deposits, the height of the sector collapse is estimated to be in the range of 5100–6500 m above the current height of 1000 m a.s.l. near the end lobe of the VDA deposits. This demonstrates that Mt. Kenya attained impressive altitudes during its main activity in the Pliocene, being one of the highest mountains in that time and was most probably covered by an ice cap. Correcting for the known net eastward tilting post eruptive uplift of approximately 500 m of the Mt. Kenya summit, our reconstruction indicates that an at least 5.6 to 7 km a.s.l. high active Mt. Kenya existed in the Pliocene landscape between 5.1 and 2.8 Ma. This volcano must have significantly contributed to regional environmental change, by catching rain on its eastern slopes and projecting a rain shadow towards the Kenya Rift valley in the west. The last major edifice collapse event around 2.8 Ma coincides with a major change in regional vegetation. This suggests that the truncating of Mt. Kenya may have caused significant changes in the local climate surrounding Mt. Kenya with possible implications for environmental change in the central Kenya Rift valley, the cradle of hominin evolution.

1. Introduction

Since the classical works of Ui (1983) and Siebert (1984) volcanic debris avalanches (VDA's) due to sector collapse of major stratovolcanoes have become more and more recognized as a common occurrence in a stratovolcano life cycle (Procter et al., 2009; Zernack et al., 2009). Most reconstructed VDA's are Holocene to recent, allowing a good characterization of their timing, origin, extent, volume, morphology and sedimentology (Ui, 1983; Siebert, 1984; Kervyn et al., 2008; Keigler et al., 2011). Older VDA's are often buried by younger events or when at the surface, have become seriously altered due to weathering and surface erosion (Mehl and Schmincke, 1999). During the last decade the sedimentology of VDA's has been more elaborated, allowing better recognition of such epiclastic breccias in the field (Bernard et al., 2009). Furthermore, improved dating techniques have suggested relations between climate and VDA's (Capra et al., 2013).

Bernard et al. (2009) distinguish debris flow deposits from VDA deposits. Their main 7 characteristics to distinguish VDA deposits are: i) thicknesses greater than 100 m, ii) mixed and block facies, iii) sharp contacts between different colour matrix components, iv) vesicles are uncommon while shattered jigsaw fracturing is common, v) massive blocks >1 m (diameter) are common, vi) shattered blocks up to 100 m in length occur and vii) large blocks of unconsolidated substratum material occur with common deformation structures.

Furthermore, at the surface a hummocky topography with lobate-shaped (convex) distal deposits is typical (Siebert, 1984; Glicken, 1996). Another morphological feature sometimes reported is the occurrence of circular depressions, which are often attributed to void collapse of melting ice blocks (Siebert, 1984; Glicken, 1996). However, since not all reported strato-volcanoes that experienced VDA's had icecaps, it seems reasonable to assume that the occurrence of such circular depressions is not a common phenomenon.

* Corresponding author at: Soil Geography and Landscape Group, Wageningen University, P.O. Box 47, NL-6700 AA Wageningen, The Netherlands.
E-mail address: Jeroen.Schoorl@wur.nl (J.M. Schoorl).

http://dx.doi.org/10.1016/j.gloplacha.2014.10.010
0921-8181/

Mt. Kenya is the remnant of a large Late Cenozoic stratovolcano (with a diameter of approximately 90 km) of predominantly phonolitic composition that lies at about 80 km East of the Kenya Rift valley (Gregory Rift, part of the large East African Rift System) on the equator. Main volcanic activity is placed in the Pliocene, with the earliest dated eruptions of Mt. Kenya already occurring around 5.8 Ma (Veldkamp et al., 2012), while the last eruption from its main vent has been dated around 2.71 Ma (Veldkamp et al., 2007; recalculated from Evernden and Curtis, 1965). More $^{40}Ar/^{39}Ar$ dates, confirming the aforementioned activity, were collected by Opdyke et al. (2010) in their attempt to reconstruct equatorial palaeomagnetic time-average field results. When we look at the Late Cenozoic volcanic stack preserved in the SE sector of Mt. Kenya, as originally mapped by Schoeman (1951), Bear (1952), Fairburn (1966), and Baker (1967), it becomes obvious that here the main volume of the exposed volcanic deposits (>95 vol.%) is made up of volcanic brecciated deposits (referred to as kenytes and phonolitic agglomerates in the older literature). The majority of these volcanic breccias are massive, heavily cemented debris deposits with many mega blocks. The remaining <5 vol.% of the preserved volcanic body consists predominantly of phonolitic lava flows. Finally, several lahars (volcanic mudflows), subdivided into 'warm' and 'cold' lahars sensus Fisher and Schmincke (1984), and associated fluvial deposits are only found in valleys downstream (Veldkamp et al., 2007; Veldkamp et al., 2012).

The similarity of these volcanic agglomerates with volcanic debris avalanches (VDA) made us hypothesise that the majority of the Mt. Kenya deposits in its SE sector are in fact volcanic debris avalanche deposits. The occurrence of one or more VDA's may have major implications for the history of Mt. Kenya because of the consequences for the associated regional climate and environmental change during the Pliocene.

It is the objective of this paper to investigate if and when debris avalanche events happened on the Pliocene Mt. Kenya. DEM analysis, field observations of sedimentary properties and surface morphology combined with $^{40}Ar/^{39}Ar$ dating, allow us to reconstruct magnitude and timing of VDA events.

2. Study area

The study area is the SE sector of Mt. Kenya located in Central Kenya and encompasses mainly the Embu and Meru districts. The general geology of the area (see Fig. 1) includes the Miocene to Pleistocene Mt. Kenya and Nyambeni volcanic deposits in the West (e.g. Baker, 1967), while a stripped Basement etch plain of Precambrian metamorphic and igneous rocks of the Mozambique Belt, is exposed in the East (Schoeman, 1951; Bear, 1952; Fairburn, 1966; Veldkamp and Oosterom, 1994). In this Basement System many NNE trending lineaments can be recognized, including the alignment of the volcanic centres on Mt. Kenya and the Nyambenis (e.g. Bear, 1952; Veldkamp et al., 2012). This and the regional tendency of the Nyambeni extrusives to become younger eastward (Brotzu et al., 1984), made Hackman et al. (1990) interpret the location of Mt. Kenya and the Nyambenis as a failed half-graben trending NE. The most comprehensive synthesis of Mt. Kenya has been published already in the 60's by Baker (1967). Since then, the main geological research emphasis has shifted towards the Kenya Rift valley (Gregory Rift System) and its closer surroundings (Smith, 1994; MacDonald, 2003).

The at present heavily dissected Mt. Kenya is overlying a high altitude tilted basement terrain (the updoming eastern shoulder of the Kenya Rift, from 900 m in the East to 2000 m in the West), with orthogneiss, migmatites and granite inselberg hills even protruding through the volcanic deposits up to altitudes of >2000 m. In the East the boundary between the Mt. Kenya breccia deposits and the Basement System area is usually a very pronounced stepped escarpment which is locally over 100 m high. In the South the transition is more gradual due to the overlying Quaternary Thiba basalts (see Fig. 1) that filled up the local topography between 0.8 and 0.45 Ma ago (Opdyke et al., 2010; Veldkamp et al., 2012). Downstream of the eastern escarpment some lower lying elongated relic plateaus of lahar and lavas overlying fluvial gravels are found (Veldkamp et al., 2007; 2012). Up to 7 major rivers, e.g. Thiba, Ena, Thuchi, Rugutti, Nithi, Mara and Mutonga are draining the humid eastern side of Mt. Kenya, all showing deeply incised gorge valleys (see Fig. 2). These rivers converge into the Tana river

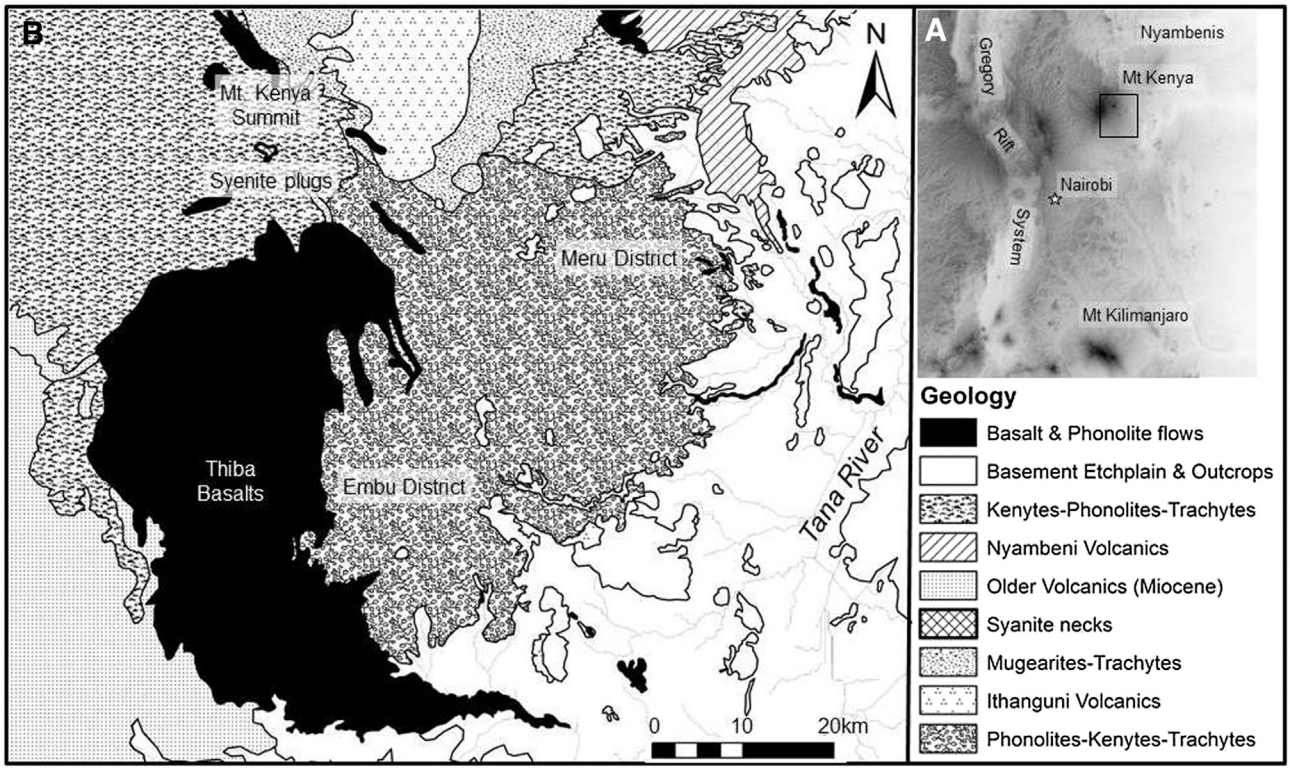

Fig. 1. Inset right A) location of the study area within Kenya in the context of the topography around the Kenya Rift System and B) simplified geology overview of the south and east sectors of Mt. Kenya, drawn after Baker (1967) and complemented with recent observations and names used in the text.

downstream, where it has incised a 160 m deep valley with gravelly fluvial strath terraces, indicating a minimum net uplift of 160 m during the last 2.65 Ma (Veldkamp et al., 2007).

The present day climate in the Mt. Kenya area is monsoonal from the southeast (2 pronounced dry and 2 wet seasons), including a strong temperature and precipitation gradient with altitude, about 1.1 C and 33 mm per 100 m, respectively (Thompson, 1966; Camberlin et al., 2014). The earlier expeditions have reported several glaciers at Mt. Kenya (Baker, 1967), at present glaciers have practically disappeared from the summit area. Nevertheless, there are multiple lines of evidence that glaciers reached down as far as below 3000 m during the Quaternary (Baker, 1967; Olago et al., 2000; Mahaney, 2011), actively accelerating the dissection of the volcano. Furthermore, we have to take into account the tropical weathering conditions and enhanced soil formation in important sections of the mountain. Since, during the Cenozoic the East African climate has become stepwise dryer (Trauth et al., 2003; Bonnefille, 2010). Consequently, during the Pliocene, a large part of East Africa was covered in tropical rainforest instead of savanna. The first drying step from forest to more grassland occurred from around 2.8 Ma (deMenocal, 2004) to 2.7 Ma BP (Bonnefille, 2010).

3. Materials and methods

3.1. Site descriptions

Fieldwork consisted of an inventory starting with previously mapped volcanic deposits (Schoeman, 1951; Bear, 1952) and discovering new outcrops during field walks (short field campaigns in 2008, 2009, 2010 and 2012). Outcrops were described when major exposures were found along road cuts, quarries and escarpments (see locations and transects in Fig. 2).

The following properties were checked when describing volcanic breccias deposits: Sorting, internal structure; Mega blocks (size, shape and monolithologic composition); jigsaw cracked blocks; induration (unconsolidated to indurated or strongly welded) and contact zones.

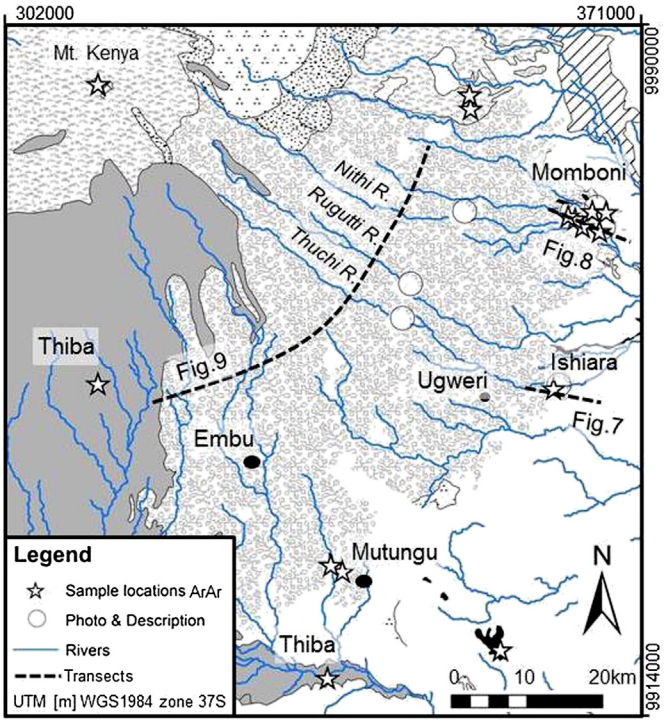

Fig. 2. Overview of the VDA fieldwork area with fieldwork locations mentioned in the text, indicated transect areas of other figures and locations of dating sample sites (see also Veldkamp et al., 2012; Opdyke et al., 2010).

All outcrops and surroundings were checked on the occurrence of fluvial sediments, tephra, lava flows and palaeosols. We used the debris flow and debris avalanche deposit key characteristics as developed by Bernard et al. (2009) to be able to distinguish them.

3.2. DEM based morphology mapping

Landscape morphology was mapped using a 30 m hole-filled seamless SRTM DEM (Reuter et al., 2007; Jarvis et al., 2008). In the field handheld GPS equipment was used to measure coordinates and altitudes. The UTM point coordinates were linked to the SRTM DEM. In this study we used the DEM altitudes for mapping altitudes, measuring gradients and to draw cross sections of selected sites.

The foot-slope area of Mt. Kenya was mapped in GIS for depressions and hummocks by processing a fill map of all local depressions and processing a multiple flow accumulation map (to identify the local waterdivides and stream network) using the LAPSUS model (Schoorl et al., 2002). Hummocks and depressions were then manually digitised by overlying the aforementioned maps over the DEM altitude and slope maps. Criteria for distinguishing real landscape depressions from DEM (stream network) inaccuracies are: i) only count depression areas of >3 grid cells of 30 m (approximately 1 ha), ii) circular features (not elongated) and iii) location separated from the local stream network (so no valley areas).

3.3. $^{40}Ar/^{39}Ar$ radio-isotopic dating

Both VDA breccia components and elongated lava flows covering VDA's were sampled for $^{40}Ar/^{39}Ar$ radio-isotopic dating (see Fig. 2 for location names and sample locations). $^{40}Ar/^{39}Ar$ incremental heating experiments on 15 samples were carried out in the geochronology laboratory at the VU University, Amsterdam. Both the phonolite lavas and VDA breccia contain large sanidine phenocrysts. The sanidine was separated using density separation in the interval 2.55–2.57 g/cm^3.

For each sample 200 mg of washed groundmass and in addition, for phonolites and VDA breccias 10 mg of sanidine was packed in 9 mm diameter Al-foil packages and loaded with packages containing a mineral standard into Al-sample containers of 20 mm diameter and 4 mm tall. The mineral standard is DRA-1 sanidine with a K/Ar age of 25.45 Ma (Wijbrans et al., 1995, recalculated as described in Kuiper et al., 2008). The sample containers were packaged in a standard Al-irradiation capsule and irradiated for 7 h in a Cd-lined rotating facility (RODEO), at the Petten HFR reactor in The Netherlands.

Upon their return to the laboratory the groundmass samples were loaded onto a 65 mm diameter Cu-sample tray that contained 5 machined depressions (3 mm deep, 17 mm diameter), and placed in a vacuum house with a 50 mm diameter multispectral ZnS window. Laser incremental heating was carried out by defocusing the laser beam to a 2 mm straight bar using an industrial scan head with a triangular deflection current of 200 Hz, and applying a fine x–y raster pattern over each of the 17 mm diameter sample positions to evenly heat the sample. For the measurement a Quadrupole mass spectrometer was used (Schneider et al., 2009). A typical mass spectrometer run consists of stepping through the argon mass spectrum from m/e:40 to m/e:35.5 at steps of a half mass unit, taking a pre-set number of digital voltmeter readings on each mass step. The beam signal on all 10 mass steps was measured on a pulse counting SEM detector.

Sanidine samples were measured using a laser single fusion technique (Kuiper et al., 2008). Aliquots of air are measured routinely during the measurement programme to monitor the mass discrimination (for a full description see Wijbrans et al., 2011). For off-line data reduction we used ArArCalc2.5 (Koppers, 2002). The ages are reported with uncertainties at 1σ following the recommendations of Renne et al. (2009).

Table 1
Description of field observation points and exposures with reference to photographs (in Figs. 3 to 5), UTMs are in [m] WGS1984 zone 37S.

Name location	UTM coordinates	Description of lithology and structures
Thuchi Bridge Fig. 3A	344713-9957112	Minimum 18 m thick exposure, no base contact, of massive, matrix-supported, polymodal and extremely poorly sorted megabreccia with mega blocks up to approx. 6 m in diameter mainly consisting out of phonolites with commonly jigsaw fracturing. Blocks of unconsolidated soil material (1.5 m) occur (Fig. 3B). Surrounding exposures infer this unit to be estimated >40 m thick.
Rugutti Fig. 3C	345603-9960861	Outcrop 12 m thick, no base contact visible, of massive matrix-supported, polymodal and extremely poorly sorted megabreccia with large phonolite blocks (>3 m in diameter, Fig. 4B). The outcrop is topped by either a phonolitic lava flow or a very large block >20 m, with a very sharp contact. Shattered jigsaw fracturing is common in smaller <2 m blocks (Fig. 3D). Blocks of unconsolidated soil material occur.
Nithi Bridge Fig. 4A	351520-9968777	At least 10 m thick outcrop, no base contact, of strongly weathered matrix-supported, polymodal and poorly sorted megabreccia with mega blocks up to approx. 2 m in diameter mainly consisting out of phonolites. Blocks of unconsolidated soil material (1.5 m) occur (Fig. 4C).
Ishiara Scarp Fig. 5A	361832-9949812	The whole unit continuous along the descending road for >90 m down. Several outcrops all minimal 8 m thick, of massive strongly matrix-supported, polymodal and extremely poorly sorted megabreccia including large blocks (>2 m), base contact overlying Basement System Gneiss including a palaeosol. Large phonolitic blocks with shattered jigsaw fracturing are common (Fig. 4D). Blocks of unconsolidated soil material were not observed. The unit is covered by a 6 m by 3 m thick phonolitic flow (sampled).
Momboni 1, 4, 5	363298-9968742 364826-9967575 366722-9967050	Total transect thickness >100 m, for all locations, surface outcrops of massive, matrix-supported, polymodal and extremely poorly sorted megabreccia with mega blocks up to approx. 2 m in diameter mainly consisting out of phonolites with commonly jigsaw fracturing. Blocks of unconsolidated soil material were not observed (Fig. 5B).
Momboni 2, 3	365932-9969244 364036-9968440	Phonolite flows with large sanidine phenocrysts with coarse columnar fracturing. The flows are lying on top as a ridge, several kilometres long, covering the underlying VDA unit (Fig. 5C).

4. Results

4.1. Outcrop description

The best available outcrops are situated along the Embu–Meru road (B6). This road constructed in 1984–1985 reveals large, now partly overgrown exposures, which extend beyond the thick tropical soil mantle. Note that in general, the volcanic area has soils up to 10 m in thickness (de Meester and Legger, 1988). These soils thin towards the generally dryer East side of Mt. Kenya, allowing rock outcrops at the surface along the transitional boundary scarp with the Basement area (e.g. de Momboni and Ishiara transects).

At the Thuchi, Rugutti and Nithi valleys, the most extensive exposures are available (see locations in Fig. 2). Outcrop descriptions and

Fig. 3. Outcrops and detailed photographs of the Mt. Kenya VDA area with A) Thuchi road outcrop with mega blocks (Dr. Schoorl and Dr. Claessens are both 1.75 m), B) Thuchi outcrop with incorporated unconsolidated materials (Dr. Schoorl is 1.75 m), C) Ruguti outcrop with mega blocks and D) Jigsaw detail from the Ruguti outcrop, hammer for scale. Locations and other specifications are given in Table 1 and Fig. 2.

Fig. 4. Photographs of the Mt. Kenya VDA outcrops and details with A) Nithi road outcrop, B) Ruguti mega block (Dr. Schoorl is 1.75 m), C) Nithi outcrop block of soil material with plant growing on it and D) Jigsaw detail from the Ishiara escarpment. Locations and other specifications are given in Table 1 and Fig. 2.

photos of the exposed deposits are presented in Table 1 and Figs. 3, 4 and 5. It is obvious from these descriptions that all the outcrop exposures along the Embu–Meru road fulfil most of the criteria for VDA deposits. All outcrops are tens of metres thick (>60 m visible at the Thuchi bridge), but never reach the basal contact. Therefore, the thicknesses in Table 1 are only minimal estimates. Outcrops consist of massive, matrix-supported, polymodal and extremely poorly sorted megabreccia with mega blocks up to approx. 6 m in diameter (mainly phonolites with commonly jigsaw fracturing and blocks of unconsolidated soil material). All visited outcrops clearly display mega blocks (Figs. 3A, C, 4B and C) and blocks of unconsolidated materials, often soil (Fig. 3B). The shattered jigsaw fracturing is visible in all outcrops as well (Figs. 3D and 4D). In all these sections only 1 VDA could be recognised, correlation is inferred by the similarity of the observations.

The exposures at the eastern escarpment zone at Ishiara and Momboni (Fig. 2) also fulfil all the criteria (Table 1, Fig. 5) with the exception that blocks with unconsolidated soil material are rare and the observed mega blocks were generally smaller in size. However, in general, the similarity of these deposits along the Embu–Meru road and the escarpment zone remain very striking, despite the fact that they are 10 to 20 km apart. Especially at the Momboni transect different geomorphological steps are evident, suggesting more than just 1 VDA event.

4.2. Morphology of the VDA unit in the SE sector of Mt. Kenya

The total VDA area is clearly distinguishable in Fig. 6A, setting off from the summit area in south-easterly direction, with the end lobes of the VDA clearly morphological expressed in the escarpment area. The surface morphology of the different VDA units (see Fig. 6B) was mapped using the SRTM DEM. Most VDA's are characterised by a hummocky relief. We have attempted to systematically map hummocks but this proved to be difficult due to the occurrence of Basement inselbergs protruding through the VDA. However, based on the DEM and Google Earth images it became apparent that the area is also characterised by many often circular bottomlands (depressions) which are often a semi-permanent wetland (see Figs. 5D and 6C). During field visits we have established that the brecciated VDA deposits are the underlying lithologies in all visited bottomlands (N > 20). It was easier to automate the mapping of these wetlands systematically for the VDA area, yielding more than 1000 bottomlands despite the heavily dissected character of the area (see overview Fig. 6B). The pattern of these depressions strongly resembles the patterns as mapped for several VDA's in Japan (Yoshida et al., 2012; their Fig. 3) and the Galunggung volcano in Java, as well as the Shasta debris avalanche (US) (e.g. Siebert, 1984). A more detailed inset (Fig. 6C) illustrates that hummocks are also visible but they are less distinct and more difficult to map. When we look at the overall map of these bottomlands (Fig. 6B) it is obvious that they occur everywhere in the unit but there are clear concentrations in the less dissected areas in the South and South East and towards the lower zones. In the more dissected area near the main rivers a similar morphology can be observed but due to local incision the bottomlands are connected to the main drainage system.

4.3. $^{40}Ar/^{39}Ar$ geochronology results

Our sampled VDA age estimates are presented in Table 2. All superimposed phonolite lava flow sanidine samples yielded acceptable $^{40}Ar/^{39}Ar$ plateau age estimates (see supplement for further discussion).

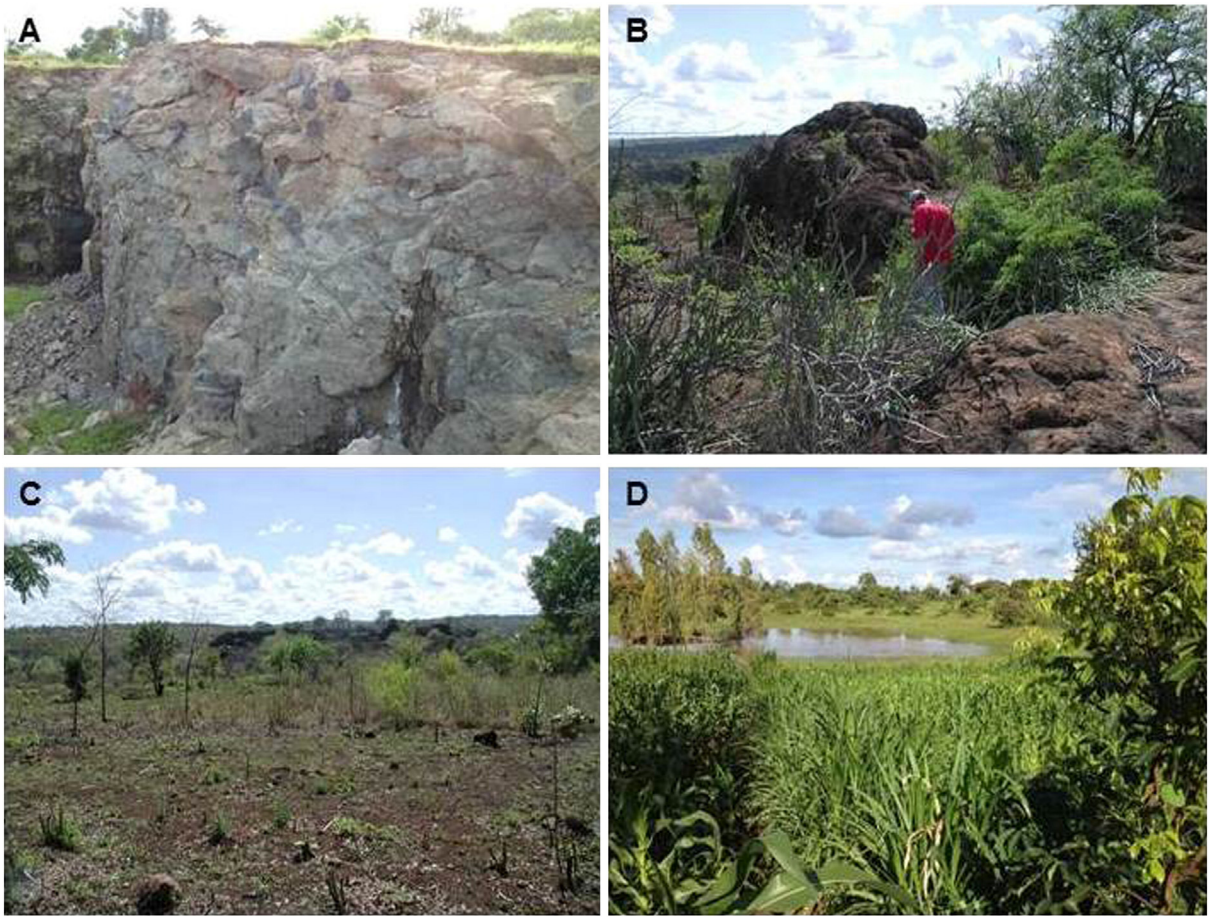

Fig. 5. Photographs of the Mt. Kenya VDA area, outcrops and details with A) Ishiara road outcrop, B) overview Momboni 4 (Prof. Veldkamp is 1.91 m), C) Momboni 1 outcrop with sealing phonolite 2 lava ridge and D) VDA depression, example of a bottomland near Ugweri. Locations and other specifications are given in Table 1, Fig. 2 and the text.

The phonolite of the Ishiara VDA III deposit yielded an age of 2.84 ± 0.01 Ma. The two Momboni phonolites are close in age yielding an age of 2.80 ± 0.01 Ma and 2.95 ± 0.02 Ma for Momboni 2 and 3, respectively.

From the brecciated VDA internal deposits both the groundmass of the breccias were measured as well as the groundmass of lava (mostly phonolite) fragments as well as sanidines extracted from the breccia and lava fragment groundmass. Given the potentially complex provenance of the VDA deposits, we propose to use the youngest estimates as the most reliable for dating the VDA-forming events. Together with the narrow age range of each section. we propose 3 different VDA events (I, II, III, from old to young, respectively). For Momboni 1 (VDA III) all four derived ages were very similar despite the various types of samples. Consequently, for Momboni 1 we propose an age of 2.82 ± 0.01 Ma. The Momboni 4 VDA II deposits display a larger range of ages. However, only the youngest age has sufficient reliable quality to use as estimate for this VDA II, yielding an age of 4.12 ± 0.05 Ma. The oldest VDA I deposit at Momboni 5 has quite a spread of ages as well but only one sample is considered to be reliable to be used as an age estimate, yielding an age of 4.94 ± 0.02 Ma. Details of age estimate quality and individual sample data are presented in a supplement.

4.4. Cross sections Mt. Kenya

Several cross sections were made to establish the relationship between morphology, stratigraphy and chronology (see Fig. 2). At the locations where $^{40}Ar/^{39}Ar$ samples were taken, Momboni and Ishiara, West–east cross-sections were made based on the SRTM DEM and field observations. In the 16 km Ishiara section (Fig. 7), an almost 200 m escarpment exists at the boundary between the VDA III deposits and the stripped etchplain developed in Basement rocks. The contact is exposed in a road cut and can be traced along the Thuchi valley several kilometres to the West. The undulating topography of the VDA III is partly due to local fluvial dissection but also due to the occurrence of local bottomlands that are temporary wetlands during the rainy seasons. Due to the uniform surface characteristics and the continuity of the outcrop along the road and Thuchi valley we infer only one VDA unit at this location (VDA III).

The 14 km Momboni section is more complex with a stepped morphology and elongated lava flows (see Fig. 8). The Nandago plateau is an isolated VDA remnant (around distance 9500 in Fig. 8) that has been dated at 4.22 ± 0.01 Ma (Veldkamp et al., 2012) based on a set of 5 different subsamples.

Following the dates as mentioned above, we distinguish in the Momboni section at least 3 different VDA deposits stacked on top if each other. The oldest VDA I (4.94 Ma) is overlain by VDA II (4.12 Ma) which in turn is covered by VDA III (2.83 Ma). All three are overlain by younger phonolite flow units of approximately 2.80 Ma. We have tentatively correlated the Nandago plateau deposit to VDA II based on morphological and age correlation, but it could also be a different VDA.

One approximately SW–NE cross section across the VDA unit was made at an equidistance of 35 km from the summit (Fig. 9, see location in Fig. 2). This cross section demonstrates a clear convex overall topography locally heavily dissected by the main rivers draining Mt. Kenya. The lower and less dissected area in the SW is the "young" Thiba basalts (0.8–0.45 Ma). The higher area between 15 and 27 km (distance along the transect), is a zone where granitoid basement inselbergs are found. These inselbergs partly protrude in the landscape but at many

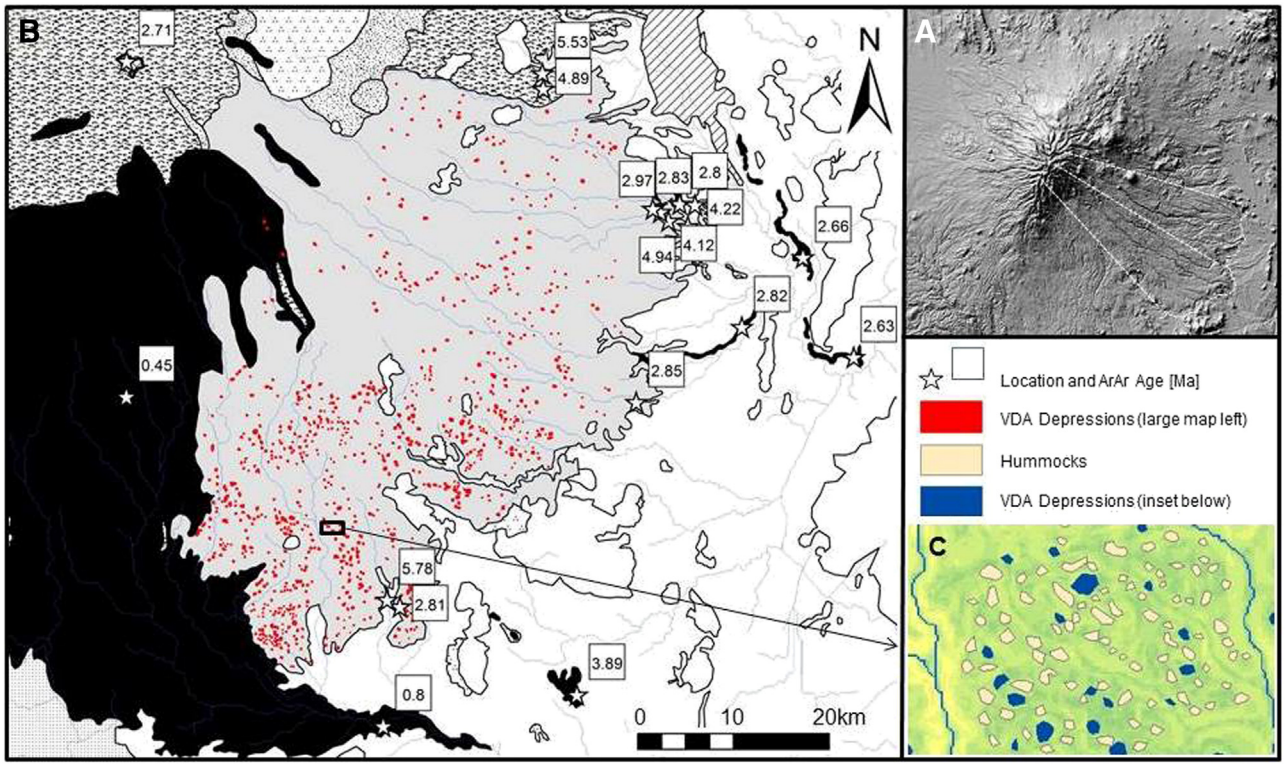

Fig. 6. Overview and detail with A) shaded relief map of Mt. Kenya (VDA area and escarpment indicated), B) overview of the VDA area with dated locations and in red the mapped depressions (large black area is the younger Thiba Basalt) and C) impression of a detailed area including bottomland depressions and hummocks. Note that location names and geological legend are given in Figs. 1 and 2. (For interpretation of the references to colour in this figure legend, the reader is referred to the web version of this article.)

locations they are covered with several metres of VDA deposits. More to the NW the VDA unit lowers down to the Muthonga river region. More to the north another volcanic unit occurs with older age estimates (4.9–5.5 Ma, Opdyke et al., 2010). Note in Fig. 9 the severe dissection along this transect by the main rivers Thuchi, Rugutti and Nithi. Consequently, as mentioned before, these valleys provided the best visible non-weathered outcrops of the VDA.

5. Discussion

5.1. Chronology

The oldest published eruptions that can be attributed to Mt. Kenya are localized trachyandesite and phonolite flows (in former valleys overlying gravel incised in Basement) with $^{40}Ar/^{39}Ar$ ages of 5.78 Ma (Veldkamp et al., 2012), 5.5–5.2 Ma (Mahaney et al., 2011) and 5.53–4.89 Ma (Opdyke et al., 2010). Based on reconstructions of the tectonic and magmatic evolution of the Kenya Rift valley it was established that between 12 and 6 Ma a halfgraben developed in the central sector. Between 5.5 and 3.7 Ma this halfgraben was antithetically faulted resulting in a full-graben morphology (Roessner and Strecker, 1997). Interestingly the initiation of Mt. Kenya volcanic activity coincides with this change in tectonic regime around 5.5 Ma. The Aberdare volcanic complex forms the eastern flank of the central rift valley and has been tilted by flank uplift to the East (Baker et al., 1988). By 2.6 Ma ago, further tectonic activity created the intra rift Kinangop plateau and a wider inner rift depression, where currently most lakes are situated (Bergner et al., 2009). Again an important change in tectonic regime coincides with, in this case, the

Table 2
Resulting (40Ar/39Ar) dates of VDA's and Phonolites, mainly Sanidines (San.), in bold the most reliable age estimates as presented in the text. Sample locations are also given in Figs. 2 and 6. Details of age estimate quality and individual dating results are presented in the supplement.

Location name	Coordinates		Height [m]	Material	Plateau age			Inv. isochr age		
	X utm	Y utm			[Ma]	1σ	MSWD	[Ma]	1σ	MSWD
Momboni 1	363298	9968742	1013	Groundmass lava	**2.82**	0.01	1.98	2.85	0.02	2.31
VDA III				Groundmass VDA	2.81	0.02	18.76	2.83	0.04	22.91
				San. Lava fragment	2.85	0.01	0.18	2.86	0.03	0.14
				San. VDA matrix	2.84	0.01	0.25	2.87	0.21	0.49
Mombini 2 (phonolite 2)	365932	9969244	926	Sanidine	**2.80**	0.01	0.94	2.77	0.03	1.07
Momboni 3 (phonolite 3)	364036	9968440	983	Sanidine	**2.95**	0.02	7.48	2.74	0.07	2.30
Momboni 4	364826	9967575	944	Groundmass lava	4.71	0.07	16.21	3.97	0.70	16.54
VDA II				Groundmass VDA	4.97	0.11	10.81	4.25	0.16	0.12
				San. Lava fragment	4.99	0.06	3.20	4.68	0.12	0.80
				San. VDA matrix	**4.12**	0.05	0.20	4.16	0.11	0.32
Momboni 5	366722	9967050	882	Groundmass Lava	4.71	0.06	11.88	4.46	0.10	3.45
VDA I				Groundmass VDA	5.15	0.03	0.46	5.23	0.24	0.24
				San. Lava fragment	4.43	0.10	9.88	4.46	0.25	15.28
				San. VDA matrix	**4.94**	0.02	0.18	4.91	0.14	0.26
Ishiara phonolite	361679	9949067	1038	Sanidine	**2.84**	0.01	1.29	2.85	0.03	1.68

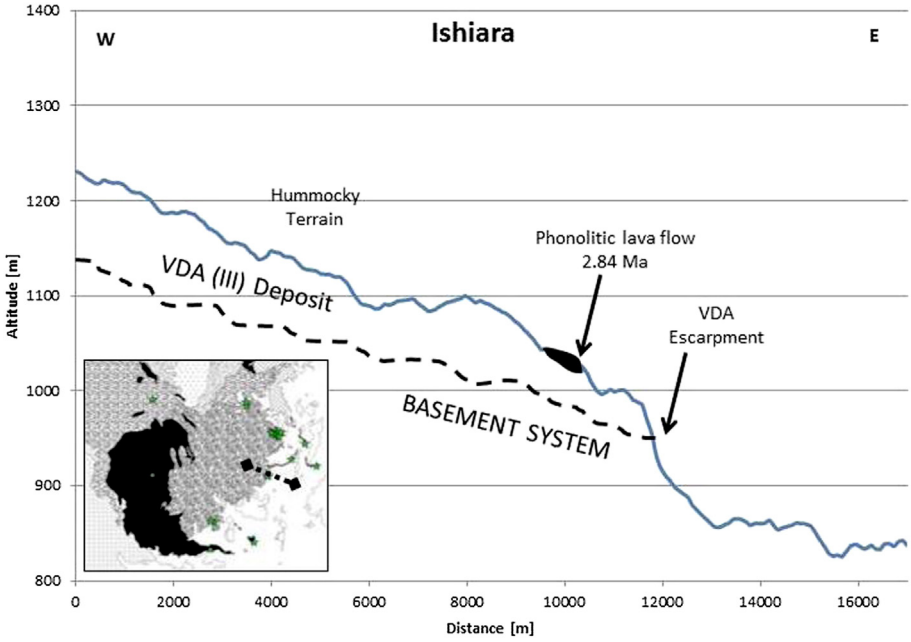

Fig. 7. Ishiara transect reconstruction of the final section of the VDA (III) in the escarpment area (see location in Fig. 2, dates in Table 2). The continuous line is the current topography, dotted line is representing a tentative VDA thickness.

termination of activity of the central vents of Mt. Kenya (2.71 Ma, Veldkamp et al., 2007).

Inferred by the stepped topography and the dated age ranges in the Momboni area (Table 2) we propose 3 different VDA's (Momboni 5, 4 and 1 from old to young). The oldest $^{40}Ar/^{39}Ar$ date in our 15 samples (Table 2) originates from a volcanic fragment found within the Momboni 5 volcanic breccias in the Mt. Kenya foot slopes and dates 5.15 Ma (Table 2), indicating the existence of an active stratovolcano erupting from the main vent during that time. This suggests a build-up of the Mt. Kenya stratovolcano already in the Miocene, between 5.8 and 5.15 Ma. We propose the oldest dated VDA (I) to be only slightly younger at 4.94 Ma. This indicates that Mt. Kenya already had constructed an edifice that collapsed after 4.94 Ma. Similar collapses occurred also about 4.12 (Momboni 4) and 2.83 Ma ago (Momboni 1 and all 3 phonolite lava flows that cover the VDA's) suggesting periodic build-up of topography and subsequent collapse. Furthermore, the three reconstructed VDA's are not localized events as their deposits have run out distances between 50 and 60 km from the main vent.

5.2. The most recent VDA

The uniform landscape morphology and a grouping of ages around 2.82 Ma suggest that the last VDA (III) which took place covered the whole SE sector during one catastrophic event. This impression is

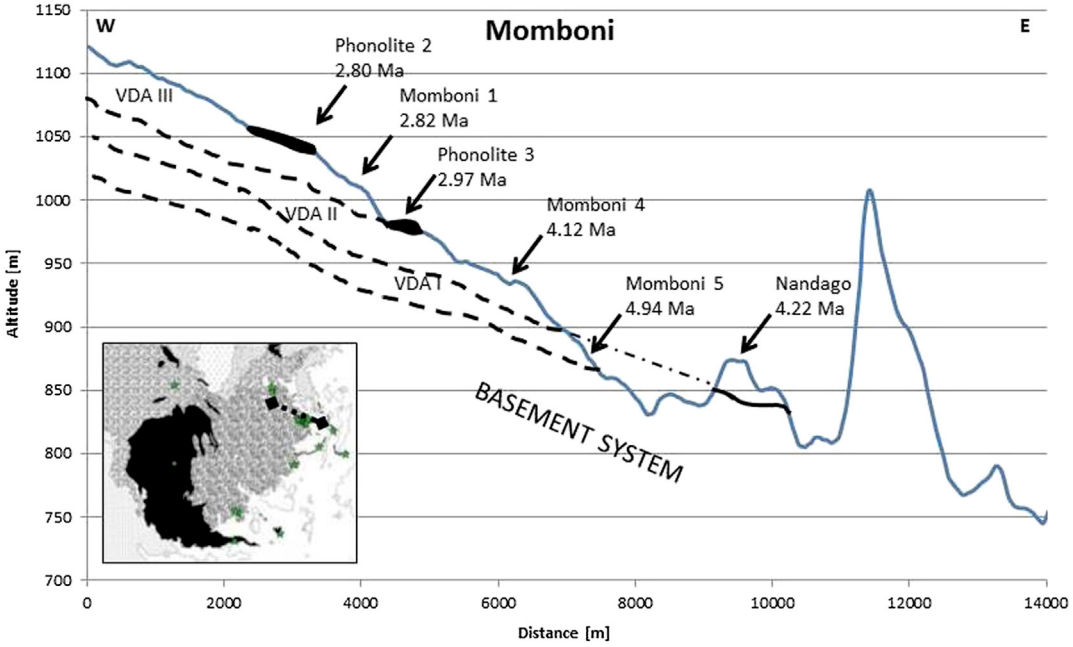

Fig. 8. Momboni transect and escarpment area including reconstruction of the end lobes of several VDA's (see location in Fig. 2, dates in Table 2). The continuous line is the current topography, different sealing lava flows are indicated. Dotted lines represent the tentative thicknesses of the different VDA's.

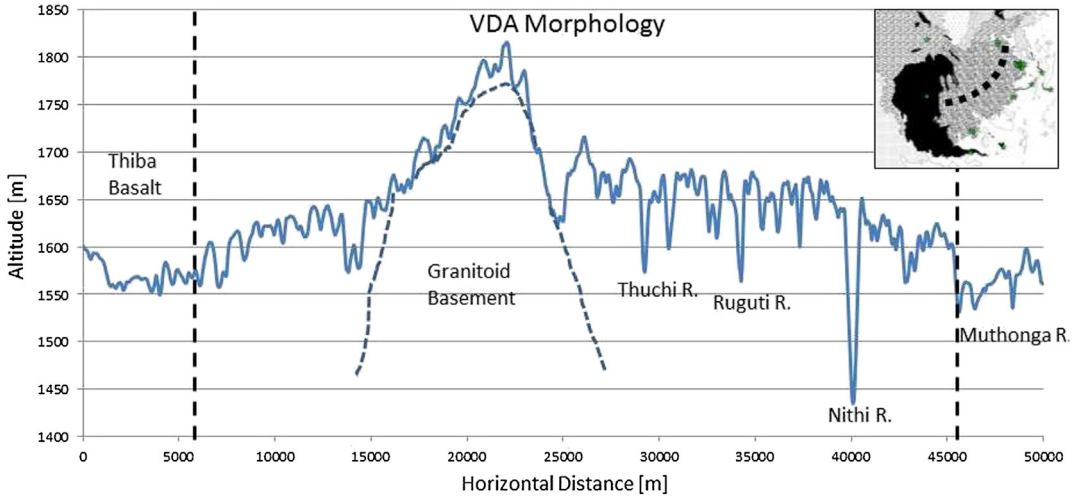

Fig. 9. Transect over the Mt. Kenya VDA mid slope area at a distance of 35 km from the summit (see location in Fig. 2). Note the lobe shape between the dashed lines (higher altitudes in the middle section) and deeply incised local river systems.

strengthened by the observation of several long elongated phonolite flows that followed the re-incised valleys of the palaeo-Thiba, Thuchi, Mutonga and Nithi rivers, which were not that deeply incised yet between 2.82 and 2.80 Ma ago. Apart from the two super imposed phonolite flows described at the Momboni section, another phonolite in the VDA yielded an age of 2.81 ± 0.01 Ma in the south near Mutungu (Veldkamp et al., 2012), as well as just outside the VDA in the palaeo Thuchi river valley (Figs. 2 and 6), where a long elongated 2.82 ± 0.01 Ma flow is found (Ugeleri, see also Veldkamp et al., 2007). Consequently, these consistent dates are found throughout the whole SE sector of Mt. Kenya. We argue that the reason that the VDA deposits in the whole area (1214 km^2) are so uniform, is due to the fact that they were formed during one huge sector collapse event. With assumed deposited thicknesses of 40 to 100 m, we are dealing with a VDA volume of 50 to 121 km^3, enough to fill a cone summit area with a radius of 10 km and 1–2 km in height. Additional evidence is presented in Baker (1967, p. 29, see his Fig. 4) where he sketches a clear concave basal contact of the youngest VDA (labelled kenyte and agglomerate). The projected VDA shear plane cuts across and above the current syenite plug (located towards the northwest), indicating a complete truncation of the summit area.

5.3. Tectonic tilting

The vast size, shape and view of the present dissected Mt. Kenya makes it hard to imagine a full sized stratovolcano in this landscape. However, a comparison of the current Mt. Kenya cross section with the younger Mt. Kilimanjaro (Nonnotte et al., 2008) suggests that Mt. Kenya is truncated and asymmetric, and is missing its whole summit and large parts of its eastern edifice including a VDA run out distance of 60 km (Fig. 10). This makes the Mt. Kenya final sector collapse one of the largest reconstructed terrestrial VDA events found to date.

The East–west cross section of Mt. Kenya in Fig. 10 demonstrates more important features. It becomes clear that the whole Mt. Kenya volcano is tilted eastward. This observation suggests a much more active Kenya Rift shoulder uplift in the Mt. Kenya and Niambeni area as compared with the area near Mt. Kilimanjaro (see also inset A Fig. 1).

Previous river gradient reconstructions based on preserved palaeogradients below lava flows to the east of Mt. Kenya indicated that this rift flank tilting also affected the Mt. Kenya area between 2.8 and 2.6 Ma (Veldkamp et al., 2007). Based on a study of the approximately 300 km long Yatta phonolite flow and modelling the emplacement history, Wichura et al. (2010) concluded that pre-rift topography

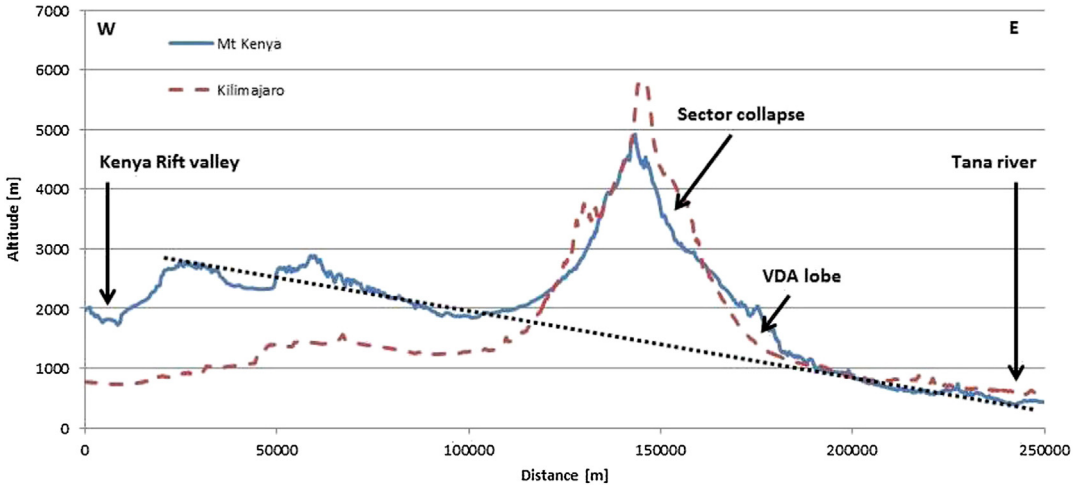

Fig. 10. Mt. Kenya cross-section (blue line): on the left the Kenya Rift valley in the West, on the right the Tana river and Basement etchplain in the East. Including comparison with a similar cross section for the Mt. Kilimanjaro area (red dashed line). Indicative sector collapse (blue under red line) and VDA depositional area (blue above redline). The dotted line gives an impression of the tectonic tilt as a consequence of the updoming rift shoulder in the Mt. Kenya area. (For interpretation of the references to colour in this figure legend, the reader is referred to the web version of this article.)

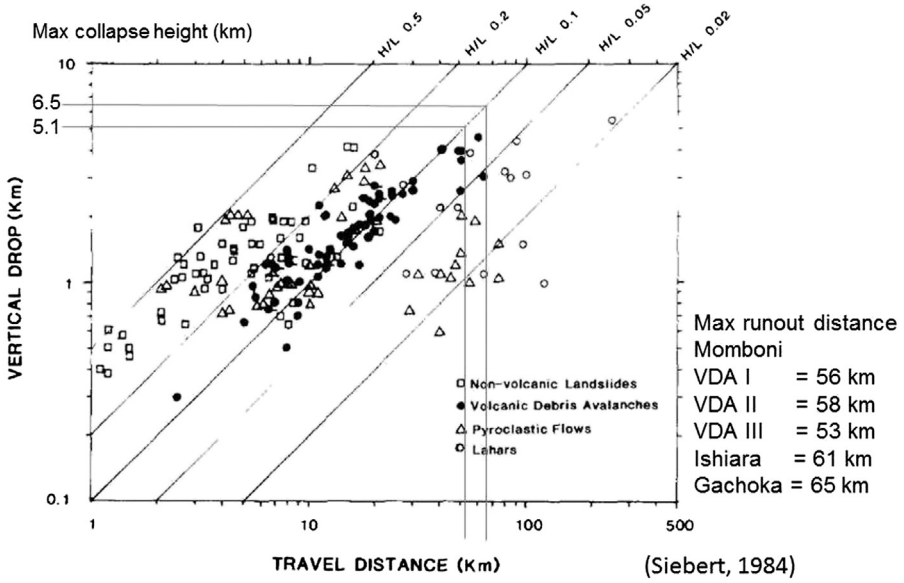

Fig. 11. Collapse height as the vertical drop vs. the travel distance or run out distance for different debris flow types (after Siebert, 1984). Plotted in blue lines on the 0.1 H\L ratio is the maximum run out distance of Mt. Kenya VDA I, II and III from the volcanic neck area to the deposits at the escarpments at Momboni (the lower left blue line) and Ishiara and Gachoka (the upper right blue line). (For interpretation of the references to colour in this figure legend, the reader is referred to the web version of this article.)

was at an altitude of approximately 1400 m during the eruption of this Yatta phonolite 13.51 Ma ago. This would suggest a net eastern rift flank uplift since that time of approximately 500 m. From the Tana river terraces we know that the post 2.65 Ma incision is approximately 180 m (Veldkamp et al., 2007). When projected on the summit of Mt. Kenya an additional uplift of at least 320 m has occurred since its activity ceased.

5.4. Reconstructing the palaeo-landscape

How high was the Mt. Kenya in the period of maximum extent as an active stratovolcano 5–2.8 Ma ago? There are two estimates already published, one based on reconstructive contour drawing yielding an estimate of 20,000 ft (6.0 km), a second estimate is based on the macrocrystallinity of the syenite plug requiring at least an additional 1 km on top, when compared to the current altitude, yielding an altitude of 6.2 km (both estimates from Baker, 1967). Our estimated VDA volume of 50 to 121 km3 is enough to fill a volcanic cone summit area with a radius of 10 km and 2 km high.

We now know that the current altitude has been elevated due to tectonic updoming. In addition, when we plot our VDA dimensions in as a debris runout or travel distance vs vertical drop or collapse height curve (Siebert, 1984), assuming here the reconstructed VDA's to have been typical of their kind with a conservative Heim coefficient of 0.1 (e.g. Siebert, 1984; Kervyn, et al., 2008; Keigler et al., 2011), we get a vertical drop of almost 5.1 to 6.5 km above the run-out altitude of the VDA deposits (now approximately 1000 m a.s.l.) yielding a projected altitude of almost 6.1 to 7.5 km (see Fig. 11). Corrected for the previously mentioned projected net post 2.8 Ma uplift of maximum 500 m, this still put the Pliocene summit of the active Mt. Kenya stratovolcano between 5.6 and 7 km above sea level.

The current snowline at Mt. Kenya is around 5 km a.s.l. and only during the last decades has the last glacier disappeared from the summit (Mahaney, 2011). If we consider that during the Pliocene it was globally 2–3° warmer (Haywood et al., 2000; Salzmann et al., 2011), the Pliocene snowline can be estimated to be at max a few hundred metres higher. Consequently, with our reconstructed Mt. Kenya altitudes of 5.6 to 7 km a.s.l., we may indeed assume considerable amounts of snow and ice at that time already on Mt. Kenya. The collapsing direction of the VDA's always to the SE is not a coincidence neither if we consider the incoming Monsoonal rains from that direction (giving more water, snow and ice in the windward area). Furthermore, we may have some additional confirmation that Mt. Kenya during the Pliocene was high enough to support an icecap (between 5.1 and 2.8 Ma) if we consider the numerous circular depressions in the VDA morphology (see previous sections and Fig. 6B) that also are reported when blocks of ice are incorporated within the VDA (e.g. Siebert, 1984; Yoshida et al., 2012).

Altogether this makes Mt. Kenya probably one of the highest mountains during this period globally. Only later during the Pliocene the Himalayas gained similar estimated altitudes (e.g. Garzione et al., 2000; Wang et al., 2012), while the Andes attained their higher altitudes only during the Quaternary (e.g. Coltorti and Ollier, 2000). In general, the continuing uplift in the Pliocene of the Kenya Rift shoulder and increasing heights of volcanic structures such as the Mt. Kenya will have enhanced orographic and orogenic effects (e.g. Roe, 2005; Strecker et al., 2007), and should be considered as possible causes for environmental change in the Mt. Kenya and Kenya Rift valley region (deMenocal, 2004).

Therefore, the existence of such a large probably ice-capped stratovolcano (between 5.1 and 2.8 Ma) must have had its effects on regional climate and vegetation zoning. Orographic precipitation effects around the Mio-Pliocene Mt. Kenya (e.g. Roe, 2005) will be directly linked to the edifice growth, trapping rain on its south eastern slopes and releasing large amounts of water to its surroundings. Consequently, the major edifice collapses that we reconstruct in this paper may have caused abrupt changes in the rainfall and water supply patterns surrounding the mountain but also in the regional patterns downwind all the way into the Kenya Rift valley. Consequently, this may have contributed to the variable environment dynamics as proposed for the 'amplifier lake theory' on environment related human evolution (Trauth et al., 2010). Consequently, our further investigations will concentrate on modelling and quantification of the probable impact on regional climate for the area around the growing and collapsing Mt. Kenya.

6. Conclusions

Our reconstruction indicates that an at least 5.6 to 7.0 km a.s.l. high active Mt. Kenya existed in the Mio-Pliocene landscape between 5.1 and 2.8 Ma, possibly one of the highest mountains on earth back then. These considerable heights infer an ice-capped summit area, enhancing the risk for lahars and volcanic debris avalanches. Consequently, Mt.

Kenya has known at least three major sector collapses resulting in different VDA events. They occurred around 4.9 Ma, 4.1 Ma and 2.83 Ma ($^{40}Ar/^{39}Ar$). The last and best preserved VDA deposit, with still some morphological expression, is presently covering the whole SE sector of 1214 km^2.

This last major edifice sector collapse event around 2.8 Ma coincides with a major change in local tectonic regimes as well as in regional vegetation. This suggests that the truncating of Mt. Kenya may have caused significant changes in environmental change around Mt. Kenya and in the central Kenya Rift valley potentially affecting hominin development.

Appendix A. Supplementary data

Supplementary data to this article can be found online at http://dx.doi.org/10.1016/j.gloplacha.2014.10.010.

References

Baker, B.H., 1967. Geology of the Mount Kenya Area, degree sheet 44 NW. Quarter, Geological Survey of Kenya, Report No. 79, Nairobi (78 pp.).

Baker, B.H., Mitchell, J.G., Williams, L.A.J., 1988. Stratigraphy, geochronology and volcanotectonic evolution of the Kedong–Naivasha–Kinangop region, Gregory Rift Valley, Kenya. J. Geol. Soc. 145, 107–116.

Bear, L.M., 1952. A geological reconnaissance of the area south-east of Embu. Geological Survey of Kenya. Report no. 23 (39 pp.).

Bergner, A.G.N., Strecker, M.R., Trauth, M.H., Deino, A., Gasse, F., Blisniuk, P., Duhnforth, M., 2009. Tectonic and climatic control on evolution of rift lakes in the Central Kenya Rift, East Africa. Quat. Sci. Rev. 28 (25–26), 2804–2816.

Bernard, B., van Wyk de Vries, B., Leyrit, H., 2009. Distinguishing volcanic debris avalanche deposits from their reworked products: the Perrier sequence (French Massif Central). Bull. Volcanol. 71, 1041–1056.

Bonnefille, R., 2010. Cenozoic vegetation, climate changes and hominid evolution in tropical Africa. Glob. Planet. Change 72 (4), 390–411.

Brotzu, P., Morbidelli, L., Nicoletti, M., Piccirillo, E.M., Traversa, G., 1984. Miocene to Quaternary volcanism in eastern Kenya: sequence and geochronology. Tectonophysics 101 (1–2), 75–86.

Camberlin, P., Boyard-Micheau, J., Philippon, N., Baron, C., Leclerc, C., Mwongera, C., 2014. Climatic gradients along the windward slopes of Mount Kenya and their implication for crop risks. Part 1: climate variability. Int. J. Climatol. 34 (7), 2136–2152.

Capra, L., Bernal, J.P., Carrasco-Núñez, G., Roverato, M., 2013. Climatic fluctuations as a significant contributing factor for volcanic collapses. Evidence from Mexico during the Late Pleistocene. Glob. Planet. Change 100, 194–203.

Coltorti, M., Ollier, C.D., 2000. Geomorphic and tectonic evolution of the Ecuadorian Andes. Geomorphology 32 (1–2), 1–19.

de Meester, T., Legger, D., 1988. Soils of the Chuka South area. Department of Soil Science and Geology Report with 4 Maps. Agricultural University, Wageningen (329 pp.).

deMenocal, P.B., 2004. African climate change and faunal evolution during the Pliocene–Pleistocene. Earth Planet. Sci. Lett. 220 (1–2), 3–24.

Evernden, J.F., Curtis, G.H., 1965. The potassium–argon dating of Late Cenozoic rocks in East Africa and Italy. Curr. Anthropol. 6, 343–385.

Fairburn, W.A., 1966. Geology of the Fort Hall area: degree sheet 44, S.W. quarter (with coloured geological map). Report 73 Geological Survey of Kenya (32 pp.).

Fisher, R.V., Schmincke, H.-U., 1984. Pyroclastic Rocks. Springer-Verlag, Berlin Heidelberg (472 pp.).

Garzione, C.N., Quade, J., DeCelles, P.G., English, N.B., 2000. Predicting paleoelevation of Tibet and the Himalaya from δ18O vs. altitude gradients in meteoric water across the Nepal Himalaya. Earth Planet. Sci. Lett. 183 (1–2), 215–229.

Glicken, H., 1996. The rockslide-debris avalanche of the May 18, 1980, Mount St. Helens Volcano, Washington. Open-File Report 96-677 U.S. Department of the Interior U.S. Geological Survey. Cascades Volcano Observatory, Vancouver, WA 98661 (90 pp., available from http://vulcan.wr.usgs.gov/Projects/Glicken/).

Hackman, B.D., Charsley, T.J., Key, R.M., Wilkinson, A.F., 1990. The development of the East African Rift system in north-central Kenya. Tectonophysics 184 (2), 189–211.

Haywood, A.M., Valdes, P.J., Sellwood, B.W., 2000. Global scale palaeoclimate reconstruction of the middle Pliocene climate using the UKMO GCM: initial results. Glob. Planet. Change 25, 239–256.

Jarvis, A., Reuter, H.I., Nelson, A., Guevara, E., 2008. Hole-Filled Seamless SRTM Data V4. International Centre for Tropical Agriculture (CIAT), (available from http://srtm.csi.cgiar.org).

Keigler, R., Thouret, J.-C., Hodgson, K.A., Neall, V.E., Lecointre, J.A., Procter, J.N., Cronin, V.E., 2011. The Whangaehu formation: debris-avalanche and lahar deposits from ancestral Ruapehu volcano, New Zealand. Geomorphology 133, 57–79.

Kervyn, M., Ernst, G.G.J., Klaudius, J., Keller, J., Mbede, E., Jacobs, P., 2008. Remote sensing study of sector collapse and debris avalanche deposits at Oldoinyo Lengai and Kermasi volcanoes, Tanzania. Int. J. Remote Sens. 29, 6565–6595.

Koppers, A.A.P., 2002. ArArCALC-software for $^{40}Ar/^{40}Ar$ age calculations. Comput. Geosci. 28, 605–619.

Kuiper, K.F., Deino, A., Hilgen, F.J., Krijgsman, W., Renne, P.R., Wijbrans, J.R., 2008. Synchronizing rock clocks of earth history. Science 320, 500–504.

MacDonald, R., 2003. Magmatism of the Kenya Rift Valley: a review. Trans. R. Soc. Edinb. Earth Sci. 93 (3), 239–253.

Mahaney, W.C., 2011. Quaternary glacial chronology of Mount Kenya massif (book). Dev. Quat. Sci. 15, 1075–1080.

Mahaney, W.C., Barendregt, R.W., Villeneuve, M., Dostal, J., Hamilton, T.S., Milner, M.W., 2011. Late Neogene volcanic and interbedded paleosols near Mount Kenya. Geol. Soc. Lond. Spec. Publ. 357, 301–318.

Mehl, K.W., Schmincke, H.-U., 1999. Structure and emplacement of the Pliocene Roque Nublo debris avalanche deposit, Gran Canaria, Spain. J. Volcanol. Geotherm. Res. 94, 105–134.

Nonnotte, P., Guillou, H., Le Gall, B., Benoit, M., Cotten, J., Scaillet, S., 2008. New K–Ar age determinations of Kilimanjaro volcano in the North Tanzanian diverging rift, East Africa. J. Volcanol. Geotherm. Res. 173 (1–2), 99–112.

Olago, D.O., Street-Perrott, F.A., Perrott, R.A., Ivanovich, M., Harkness, D.D., 2000. Late Quaternary primary tephras in Sacred Lake sediments, northeast Mount Kenya, Kenya. J. Afr. Earth Sci. 30 (4), 957–969.

Opdyke, N.D., Kent, D.V., Huang, K., Foster, D.A., Patel, J.P., 2010. Equatorial paleomagnetic time-averaged field results from 0–5 Ma lavas from Kenya and the latitudinal variation of angular dispersion. Geochem. Geophys. Geosyst. 11 (5), 1–20.

Procter, J.N., Cronin, S.J., Zernack, A.V., 2009. Landscape and sedimentary response to catastrophic debris avalanches, western Taranaki, New Zealand. Sediment. Geol. 220, 271–287.

Renne, P.R., Deino, A.L., Hames, W.E., Heizler, M.T., Hemming, S.R., Hodges, K.V., Koppers, A.A.P., Mark, D.F., Morgan, L.E., Phillips, D., Singer, B.S., Turrin, B.D., Villa, I.M., Villeneuve, M., Wijbrans, J.R., 2009. Data reporting norms for $^{40}Ar/^{39}Ar$ geochronology. Quat. Geochronol. 4 (5), 346–352.

Reuter, H.I., Nelson, A., Jarvis, A., 2007. An evaluation of void filling interpolation methods for SRTM data. Int. J. Geogr. Inf. Sci. 21 (9), 983–1008.

Roe, G.H., 2005. Orographic precipitation. Annu. Rev. Earth Planet. Sci. 33, 645–671.

Roessner, S., Strecker, M.R., 1997. Late Cenozoic tectonics and denudation in the Central Kenya Rift: quantification of long-term denudation rates. Tectonophysics 278 (1–4), 83–94.

Salzmann, U., Williams, M., Haywood, A.M., Johnson, A.L.A., Kender, S., Zalasiewicz, J., 2011. Climate and environment of a Pliocene warm world. Palaeogeogr. Palaeoclimatol. Palaeoecol. 309, 1–8.

Schneider, B., Kuiper, K., Postma, O., Wijbrans, J., 2009. $^{40}Ar/^{39}Ar$ geochronology using a quadrupole mass spectrometer. Quat. Geochronol. 4, 508–516.

Schoeman, J.J., 1951. A geological reconnaissance of the country between Embu and Meru. Geological Survey of Kenya, 1:125,000 map. Report No. 17, Nairobi. 57 pp.

Schoorl, J.M., Veldkamp, A., Bouma, J., 2002. Modeling water and soil redistribution in a dynamic landscape context. Soil Sci. Soc. Am. J. 66 (5), 1610–1619.

Siebert, L., 1984. Large volcanic debris avalanches: characteristics of source areas, deposits and associated eruptions. J. Volcanol. Geotherm. Res. 22, 163–197.

Smith, M., 1994. Stratigraphic and structural constraints on mechanism of active rifting in the Gregory rift, Kenya. Tectonophysics 236, 3–22.

Strecker, M.R., Alonso, R.N., Bookhagen, B., Carrapa, B., Hilley, G.E., Sobel, E.R., Trauth, M.H., 2007. Tectonics and climate of the southern central Andes. Annu. Rev. Earth Planet. Sci. 35, 747–787.

Thompson, B.W., 1966. The mean annual rainfall of Mount Kenya. Weather 21, 48–49.

Trauth, M.H., Deino, A.L., Bergner, A.G.N., Strecker, M.R., 2003. East African climate change and orbital forcing during the last 175 kyr BP. Earth Planet. Sci. Lett. 206 (3–4), 297–313.

Trauth, M.H., Maslin, M.A., Deino, A.L., Junginger, A., Lesoloyia, M., Odada, E.O., Olago, D.O., Olaka, L.A., Strecker, M.R., Tiedemann, R., 2010. Human evolution in a variable environment: the amplifier lakes of Eastern Africa. Quat. Sci. Rev. 29 (23–24), 2981–2988.

Ui, T., 1983. Volcanic dry avalanche deposits — identification and comparison with non-volcanic debris stream deposits. J. Volcanol. Geotherm. Res. 18, 135–150.

Veldkamp, A., Oosterom, A.P., 1994. The role of episodic plain formation and continuous etching and stripping processes in the End-Tertiary landscape development of SE Kenya. Z. Geomorphol. 38, 75–90.

Veldkamp, A., Buis, E., Wijbrans, J.R., Olago, D.O., Boshoven, E.H., Marée, M., van den Berg van Saparoea, R.M., 2007. Late Cenozoic fluvial dynamics of the River Tana, Kenya, an uplift dominated record. Quat. Sci. Rev. 26, 2897–2912.

Veldkamp, A., Schoorl, J.M., Wijbrans, J.R., Claessens, L., 2012. Mount Kenya volcanic activity and the Late Cenozoic landscape reorganisation in the upper Tana fluvial system. Geomorphology 145–146, 19–31.

Wang, Y., Deng, T., Flynn, L., Wang, X., Yin, A., Xu, Y., Parker, W., Lochner, E., Zhang, C., Biasatti, D., 2012. Late Neogene environmental changes in the central Himalaya related to tectonic uplift and orbital forcing. J. Asian Earth Sci. 44, 62–76.

Wichura, H., Bousquet, R., Oberhaensli, R., Strecker, M.R., Trauth, M.H., 2010. Evidence for middle Miocene uplift of the East African Plateau. Geology 38 (6), 543–546.

Wijbrans, J.R., Pringle, M.S., Koppers, A.A.P., Scheveers, R., 1995. Argon geochronology of small samples using the vulkaan argon laserprobe. Proc. K. Ned. Akad. W. Biol. Chem. Geol. Phys. Med. Sci. 98 (2), 185–218.

Wijbrans, J., Schneider, B., Kuiper, K., Calvari, S., Branca, S., De Beni, E., Norinic, G., Corsaro, R.A., Miraglia, L., 2011. $^{40}Ar/^{39}Ar$ geochronology of Holocene basalts; examples from Stromboli, Italy. Quat. Geochronol. 6 (2), 223–232.

Yoshida, H., Sugai, T., Ohmori, H., 2012. Size–distance relationships for hummocks on volcanic rockslide-debris avalanche deposits in Japan. Geomorphology 136, 76–87.

Zernack, A.V., Procter, J.N., Cronin, S.J., 2009. Sedimentary signatures of cyclic growth and destruction of stratovolcanoes: a case study from Mt. Taranaki, New Zealand. Sediment. Geol. 220, 288–305.